

Optical Möbius Singularities

Isaac Freund

Physics Department, Bar-Ilan University, Ramat-Gan ISL52900, Israel

Möbius strips with one, two, three, and four, half-twists are shown to be generic features of three-dimensional (nonparaxial) elliptically polarized light. The geometry and topology of these unusual singularities is described and the multitude of winding numbers that characterize their structures is enumerated; probabilities for the appearance of different configurations are presented.

PACS numbers: 42.25.-p, 42.25.Dd, 42.25.Ja

The singularities of optical fields are major determinants of the field structure that are of intense current interest [1 – 13]. Here we extend previous studies of polarization singularities in three dimensional (3D) optical fields [14 – 22], finding new, highly unusual structures.

3D light, i.e. light composed of waves with a broad spread of noncoplanar propagation directions, is almost invariably elliptically polarized. The generic singularities of 3D optical (and other electromagnetic) ellipse fields are lines of circular polarization, C lines, and lines of linear polarization, L lines [19 – 22]. At the point where a C line (L line) pierces a plane, Σ , a C point (L point) appears. The principal axes of the polarization ellipse are the major axis, the minor axis, and the ellipse normal. At a C point the ellipse degenerates into a circle, the C circle, and the major and minor axes are undefined (singular). At an L point the ellipse collapses to a line, the major axis of the ellipse, and the minor axis of, and the normal to, the ellipse become undefined.

All three principal axes of the ellipses surrounding the singularity, however, remain well defined. The projections onto Σ of the major and minor axes (minor axis and normal) of those ellipses whose centers lie in this plane rotate about the C point (L point) with characteristic winding number $\pm 1/2$ (± 1) [19 – 22]. Throughout this report, for C points (L points) we take Σ to be the plane of the C circle (to be oriented perpendicular to the major axis). We call this plane the *principal plane*, and label it Σ_0 .

Previous studies of 3D light have concentrated on projections onto the principal plane Σ_0 of the polarization ellipses whose centers lie in this plane; here we study the *full* 3D arrangement of these ellipses. Choosing for simplicity concentric circular paths in Σ_0 that surround a C or L point, we find that for $\sim 80\%$ of all C points both the major and minor axes of the ellipses on each path generate a Möbius strip with a single half twist, whereas for the remaining 20% the Möbius strip has three half twists. Möbius strips on paths surrounding L points are generated both by the minor axes of, and the normals to, the surrounding ellipses, and have two full twists. Previously [14], we showed that the polarization ellipses surrounding ordinary (nonsingular) points generate Möbius strips with one full twist, so that together with the results reported here, the polarization ellipses in 3D electromagnetic fields generically produce Möbius strips with one

half-, two half-, three half-, and four half-twists. Representative Möbius strips are shown in Fig. 1.

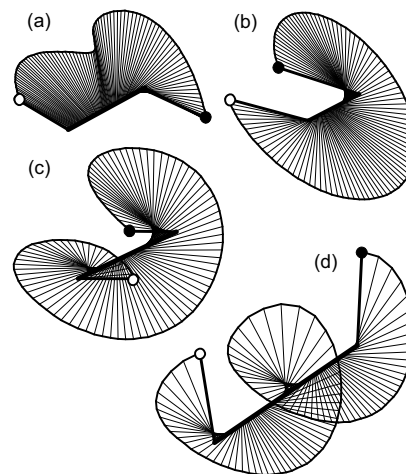


FIG. 1: Optical Möbius singularities in a random ellipse field. For clarity, the Möbius strips formed by the polarization ellipses whose centers lie on a small circle in Σ_0 are opened and straightened. Ellipse axes are shown by the thin straight lines that spiral around the thick straight line formed by the ellipse centers; only the upper half of each axis is shown. The small white (black) circle marks the ellipse at the arbitrary “beginning” (“end”) of the opened Möbius strip; when the strip is closed these two ellipses are adjacent. For an odd (even) number of half twists the white and black circles are on opposite sides (the same side) of the line of ellipse centers. (a)-(d) Möbius strips formed by the major axes (a)-(c) or ellipse normals (d) of the polarization ellipses surrounding: (a) a C point - this (wrinkled) strip has a single half twist; (b) an ordinary (nonsingular) point - this strip has one full twist; (c) a C point that is different from the one in (a) - this strip has three half twists; (d) an L point - this strip has two full twists. The Möbius strip in (a) forms a right-handed screw and has topological index $-1/2$, the strips in (b) - (d) form left-handed screws and have indices $+1$, $+3/2$, and $+2$, respectively. In random fields right/left-handed strips occur with equal probabilities. Although a circular path is chosen here for simplicity, any simple path that encloses only the C or L point yields (a possibly highly wrinkled) Möbius strip with the same twist index as does the circle

Simple physical models of Möbius strips with the same topology as those in Fig. 1 can be constructed from short thin rods and a long strip of somewhat flexible material.

For a model of a C point (L point) the rods represent say the major axis (ellipse normal). The “upper” half of each rod is painted black, the rods are oriented parallel to one another and attached at their centers to the flexible strip such that they are perpendicular to the long axis of the strip. Introducing the appropriate number of half twists generates a model of the desired figure in Fig. 1; gluing the ends of the strip together completes the construction of a model of the Möbius strip that surrounds a C or an L point.

By continuity, for C points (L points) the angle that say the major axis (ellipse normal) of the surrounding ellipses makes with the principal plane goes to zero as one approaches the central singularity. In the physical model described above this can be accomplished simply by squashing the Möbius strip flat. Such a deformation changes the geometry of the strip but preserves its topology; the deformations in real optical ellipse fields are, of course, rather more subtle.

In optical ellipse fields there are no packing problems due to overlap of the axes of neighboring ellipses in the concentric, nested Möbius strips surrounding C and L points. The reason is that the polarization ellipse describes the time variation of the oscillating electric field at a point, so that the ellipse has dimension zero, whereas the Möbius strip has dimension one, and is a line.

The Möbius strips in Fig. 1 were measured in a simulated 3D random optical field (speckle pattern), where the optical field, \mathbf{E} , in complex representation, was generated as a sum of 100 plane waves with random phases and randomly oriented transverse linear polarizations. Many waves, however, are not required for C and L lines and their Möbius strips; all these features are found in three beam optical lattices.

The C and L lines used in Fig. 1 were obtained from the above simulation by tracking zeros of the C and L point discriminants $D_C = a_1^2 - 4a_2$, and $D_L = a_2$; these discriminants are obtained from the characteristic equation $\lambda^2 + a_1\lambda + a_2 = 0$ of the real coherency matrix $M_{ij} = \text{Re}(E_i^* E_j)$; $i, j = x, y, z$ [16]. The orientation of the major axis α and the minor axis β of the ellipses surrounding a C or L point were calculated using formulas due to Berry [15, 18]: $\alpha = \text{Re}(\mathbf{E}^* \sqrt{\mathbf{E} \cdot \mathbf{E}})$, $\beta = \text{Im}(\mathbf{E}^* \sqrt{\mathbf{E} \cdot \mathbf{E}})$; the normal to the ellipse, γ , was calculated using $\gamma = \text{Im}(\mathbf{E}^* \times \mathbf{E})$ [19].

The three primary topological indices that characterize a C point in a 3D field are: (i) The well known [19] winding number $I_\alpha^{(C)} \equiv I_\beta^{(C)} = \pm 1/2$ of the projection onto the principal plane Σ_0 of the major or minor axes of the surrounding ellipses; (ii) The winding number $I_\gamma^{(C)} = \pm 1$ (not discussed previously) of the projection onto Σ_0 of the normals to the surrounding ellipses; and (iii) the first of the two major findings of this report: the twist index $\tau_\alpha^{(C)} = \tau_\beta^{(C)} = \pm 1/2, \pm 3/2$ of the Möbius strips generated by the major and minor axes of the surrounding ellipses. For C points, axis γ does not generate a Möbius strip. The above three indices generate $2 \times 2 \times 4 = 16$ different

C points, an eight-fold enlargement of previous C point characterizations [19]. All 16 C points appear in our simulations; $\tau_\alpha^{(C)}$ is illustrated in Fig. 1, $I_\alpha^{(C)}$ and $I_\gamma^{(C)}$ are illustrated in Fig. 2.

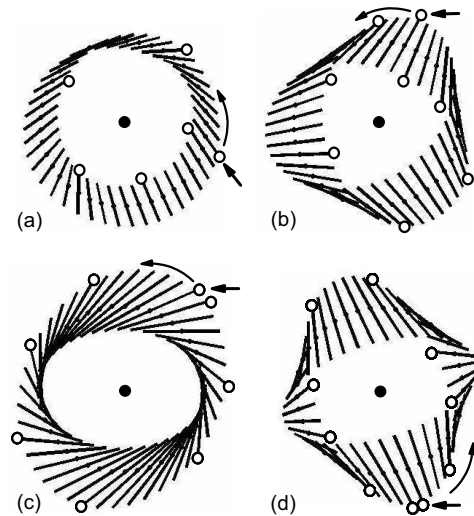


FIG. 2: C point indices $I_\alpha^{(C)}$ and $I_\gamma^{(C)}$. $I_\alpha^{(C)}$ ($I_\gamma^{(C)}$) is generated by the projections onto the principal plane Σ_0 of axis α (axis γ) of the ellipses surrounding the C point. Conventionally, the centers of the surrounding ellipses are taken to be located on a small circle surrounding the C point, although any simple closed path produces the same index. Projections of the axes of the surrounding ellipses onto Σ_0 are shown by short straight lines, ellipse centers by small black dots, and the C point by the central black circle. As an aid in following the rotation of the axes one end is decorated by a small white circle. The here counterclockwise direction in which the surrounding circle (path) is traversed is shown by a curved arrow, the starting point of the path by a small straight arrow. (a) $I_\alpha^{(C)}$ for the C point in Fig. 1(a). The net rotation of the ellipse axes is in the same counterclockwise direction as the path, so the sign of $I_\alpha^{(C)}$ is positive. The axes rotate by 180° during one 360° traverse of the path, so the magnitude of the winding number is $1/2$. Adding in the sign, yields $I_\alpha^{(C)} = +1/2$. (b) $I_\alpha^{(C)}$ for the C point in Fig. 1(c). The ellipses rotate by 180° in the clockwise (retrograde) direction and $I_\alpha^{(C)} = -1/2$. (c) $I_\gamma^{(C)}$ for the C point in Fig. 1(a). The ellipses rotate by 360° in the same clockwise direction as the path and $I_\gamma^{(C)} = +1$. $I_\gamma^{(C)} = +1$ also for the C point in Fig. 1(c). (d) $I_\gamma^{(C)}$ for another ellipse located on the same C line as the ellipse in Fig. 1(c). Here $I_\gamma^{(C)} = -1$.

The complex field components E_x , E_y , and E_z , in the immediate vicinity of any point in a 3D field can be expanded to first order (the order required here) as $E_m = K_m + \sum_{n=x,y,z} (P_{mn} + iQ_{mn}) u_n$, where $m = x, y, z$, and $u_x = x$, $u_y = y$, $u_z = z$. Without loss of generality, for C points we take K_x to be real, set $K_y = i\sigma |K_x|$, where $\sigma = \pm 1$, and set $K_z = 0$ and $u_z = z = 0$. This describes a C point at the origin with the normal to the C circle oriented along the z -axis, and the surrounding ellipses lying in the principal plane Σ_0 of the C point, here the xy -

plane. Similarly, for L points we take K_z to be real, set $K_x = K_y = 0$ and $u_z = z = 0$. This describes an L point at the origin with its major axis oriented along the z -axis, and again places the surrounding ellipses in the xy -plane, the principal plane Σ_0 of the L point. In both cases, in the principal plane Σ_0 , the generally nonzero parameters P_{nz} and Q_{nz} make no contribution because their multiplier, z , is zero. The field component E_z is not zero, however, because it involves terms in x and y that are not zero. We note that all structures found in our simulations were reproduced using this expansion with suitable choices for the expansion parameters K, P, Q . Analytical expressions can be obtained for the various indices in terms of these expansion parameters by extending the methods of [14]; these methods require a discussion that is too lengthy to be included here.

Close facsimiles of the measured random field strips in Fig. 1 can be generated from simpler expansions. The Möbius strip in Fig. 1(a), for example, is reasonably well approximated by $Ex = -5 + y(i - 1)$, $Ey = -5i + x$, $Ez = -ix + y$; that in Fig. 1(b) by $Ex = -5$, $Ey = i$, $Ez = -y$; the one in Fig. 1(c) by $Ex = 10 - y$, $Ey = 10i - x$, $Ez = y$; and the strip in Fig. 1(d) by $Ex = i(2y - x)$, $Ey = x + iy$, $Ez = 5$.

Preliminary statistics of the various topological indices were obtained by choosing random values for the nonzero K , the various P and Q , and the sign of σ . A random number generator that produced a normal distribution with unit variance was used. The data listed below were obtained from 1.6×10^6 independent samples.

Fig. 3 presents a modified Zipf plot for the three C point indices $I_\alpha^{(C)}$, $I_\gamma^{(C)}$, and $\tau_\alpha^{(C)}$.

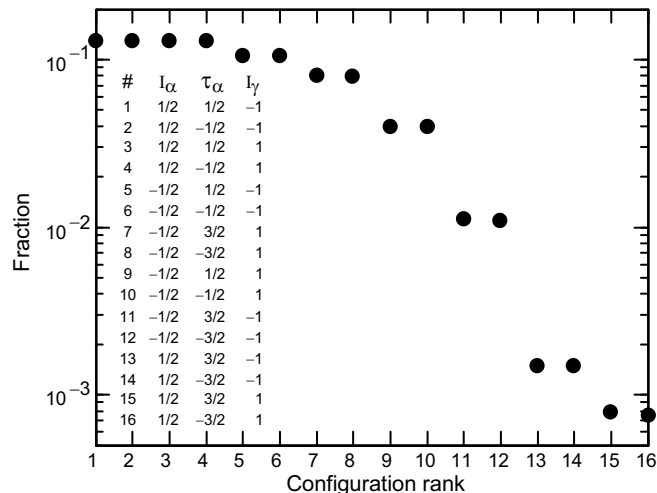


FIG. 3: C point Zipf plot. Configuration fraction (probability) vs. configuration rank for configurations ranked by decreasing probabilities.

There are four primary topological indices that characterize an L point. The first two indices are the well known [19] winding number $I_\beta^{(L)} \equiv I_\gamma^{(L)} = \pm 1$, and the index $I_\alpha^{(L)} = \pm 1$ (not discussed previously). These in-

dicies are analogous to the corresponding C point indices $I_\alpha^{(C)} \equiv I_\beta^{(C)}$, and $I_\gamma^{(C)}$. The other two indices are the second major finding of this report: the two independent twist indices, $\tau_\beta^{(L)} = \pm 2$, and $\tau_\gamma^{(L)} = \pm 2$. The Möbius strip in Fig. 1(d) was generated by axis γ and has index $\tau_\gamma^{(L)} = +2$, whereas the strip generated by axis β for the same L point has index $\tau_\beta^{(L)} = -2$. For L points, axis α does not generate a Möbius strip.

These four L point indices generate $2^4 = 16$ different L points, all of which appear in our simulations. Fig. 4 presents a modified Zipf plot that summarizes the different L point configurations and their relative probabilities.

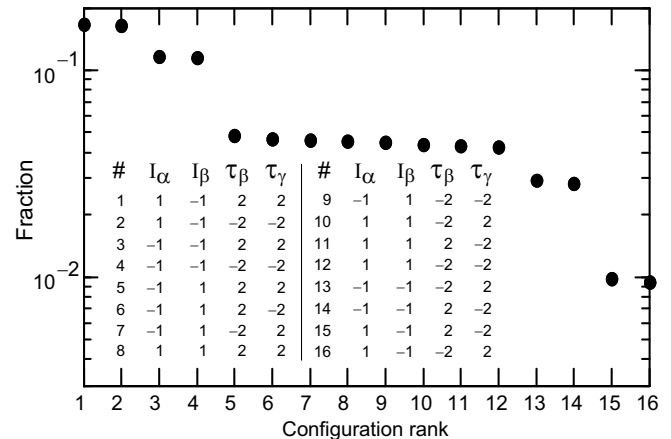


FIG. 4: L point Zipf plot.

There are four geometrically distinct types of L points. We label these L_{mm} , L_{mc} , L_{cm} , and L_{cc} , where the first subscript refers to the figure generated by axis β of the surrounding ellipses, the second to axis γ ; m (c) implies that the figure is a Möbius strip (“cone”). The differences between Möbius strips and cones are shown in Fig. 5. Although it is relatively easy to distinguish visually between Möbius strips and cones, it is difficult to do so with complete reliability using a computer program. From visual examination of some 100 L points we observed that L_{mm} points appear mostly, but not exclusively, for negative $I_\beta^{(L)}$ and L_{cc} points appear mostly, but not exclusively, for positive $I_\beta^{(L)}$; L_{mc} and L_{cm} points appear less frequently than do L_{mm} and L_{cc} points. The data in Fig. 4 do not distinguish between topological equivalent but geometrically distinct L points: this figure lists all L points with a given index configuration without regard to whether these points are L_{mm} , L_{mc} , L_{cm} , or L_{cc} .

The topological indices discussed here are all of first order in the sense that the field modulations that give rise to them grow linearly with distance from the singularity; these indices should be observable in microwave [3, 4, 20] and in interferometric, phase-sensitive, nanoprobe optical [23–27] experiments that are able to probe the three-dimensional structure of the field.

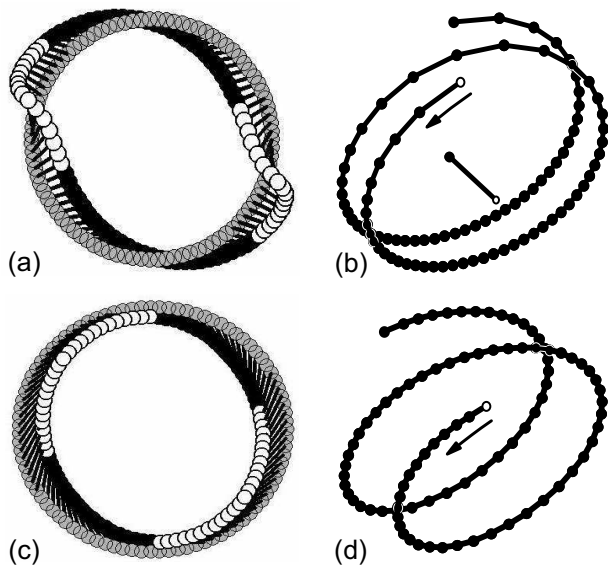


FIG. 5: L point structures. The ellipses in Σ_0 that surround an L point can generate one of two geometrically distinct structures: (a),(b) a double-full-twist Möbius strip, or (c),(d) a section of a cone. Ellipse half-axes of the surrounding ellipses are shown by thick straight lines, the centers of these ellipses by light gray circles; the L point itself (not shown) lies at the center of this circle. The end points of the ellipse axes are shown by filled white (black) circles if these endpoints lie above (below) the plane of ellipse centers. In (a) the ellipse endpoints wind around the circle of ellipse centers to form a pair of interlocking rings. This Möbius strip is the one shown in Fig. 1(d). As shown here in (b), an observer walking along the circle of ellipse centers sees the endpoints spiral around her path (central straight line); the winding number of this spiral is $\tau = +2$. In (c) the endpoint circle and the circle of ellipse centers do not interlock, and this structure is not a Möbius strip. An observing walking along the circle of ellipse centers sees a section of an inverted cone whose "bottom" edge is her path and whose "top" edge, formed by the ellipse endpoints, is fluted and deeply scalloped; these endpoints form the spiral in (d), which has winding number $\tau = +2$. Inverted cones, such as the one shown here, and cones in which the ellipse axes flare outward, instead of inward, from the circle of ellipse centers are equally probable, as are positive (+2) and negative (-2) values for τ .

C and L lines and their associated C and L points correspond to degeneracies of symmetric second order tensors (matrices) [17, 18]. Accordingly, they, and their associated Möbius strips, can be expected to occur, and should therefore be sought, in other physical line and vector fields described by such tensors; candidates include liquid crystals, strain fields, and flow fields.

I thank Prof. David A. Kessler for helpful comments and suggestions.

[1] R. I. Egorov, M. S. Soskin, D. A. Kessler, and I. Fre-

und, Phys. Rev. Lett. **100**, 103901 (2008).

[2] K. O'Holleran, M. R. Dennis, F. Flossmann, and M. J. Padgett, Phys. Rev. Lett. **100**, 053902 (2008).

[3] S. Zhang and A. Z. Genack, Phys. Rev. Lett. **99**, 203901 (2007)

[4] S. Zhang, B. Hu, P. Sebbah, and A. Z. Genack, Phys. Rev. Lett. **99**, 063902 (2007).

[5] R. Pugatch, M. Shuker, O. Firstenberg, A. Ron, and N. Davidson, Phys. Rev. Lett. **98**, 203601 (2007).

[6] O. Peleg, G. Bartal, B. Freedman, O. Manela, M. Segev, and D. N. Christodoulides, Phys. Rev. Lett. **98**, 103901 (2007).

[7] W. Wang, Z. Duan, S. G. Hanson, Y. Miyamoto, and M. Takeda, Phys. Rev. Lett. **96**, 073902 (2006).

[8] Y. F. Chen, T. H. Lu, and K. F. Huang, Phys. Rev. Lett. **96**, 033901 (2006).

[9] F. Flossmann, U. T. Schwarz, M. Maier, and M. R. Dennis, Phys. Rev. Lett. **95**, 253901 (2005).

[10] H. F. Schouten, T. D. Visser, G. Gbur, D. Lenstra, and H. Blok, Phys. Rev. Lett. **93**, 173901 (2004).

[11] G. A. Swartzlander, Jr. and J. Schmit, Phys. Rev. Lett. **93**, 093901 (2004).

[12] D. M. Palacios, I. D. Maleev, A. S. Marathay, and G. A. Swartzlander, Jr., Phys. Rev. Lett. **92**, 143905 (2004).

[13] D. R. Solli, C. F. McCormick, R. Y. Chiao, S. Popescu, and J. M. Hickmann, Phys. Rev. Lett. **92**, 043601 (2004).

[14] I. Freund, Opt. Commun. **256**, 220 (2005); *ibid* **249**, 7 (2005).

[15] M. V. Berry, J. Opt. A **6**, 675 (2004).

[16] I. Freund, J. Opt. A **6**, S229 (2004).

[17] M. V. Berry and M. R. Dennis, Proc. Roy. Soc. Lond. A **457**, 141 (2001).

[18] M. V. Berry in *Singular Optics 2000*, ed. M. S. Soskin, Proc. SPIE **4403**, 1 (2001).

[19] J. F. Nye, *Natural Focusing and Fine Structure of Light* (IOP Publ., Bristol, 1999).

[20] J. V. Hajnal, Proc. Roy. Soc. Lond. A **430**, 413 (1990); *ibid* **447** (1987); *ibid* **414**, 433 (1987).

[21] J. F. Nye and J. V. Hajnal, Proc. Roy. Soc. Lond. A **409**, 21 (1987).

[22] J. F. Nye, Proc. Roy. Soc. Lond. A **389**, 279 (1983); *ibid* **387**, 105 (1983).

[23] Z. H. Kim and S. R. Leone, Opt. Express **16**, 1733 (2008).

[24] K. G. Lee, H. W. Kihm, J. E. Kihm, W. J. Choi, H. Kim, C. Ropers, D. J. Park, Y. C. Yoon, S. B. Choi, D. H. Woo, J. Kim, B. Lee, Q. H. Park, C. Lienau, D. S. Kim, Nature Photon. **1**, 53 (2006).

[25] C. Rockstuhl, I. Marki, T. Scharf, M. Salt, H. P. Herzig, and R. Dandliker, Current Nanoscience **2**, 337 (2006).

[26] R. Dandliker, I. Marki, M. Salt, and A. Nesci, J. Opt. A. **6**, S189 (2004).

[27] M. L. M. Balistreri, H. Gersen, J. P. Korterik, L. Kuipers, and N. F. van Hulst, Science **294**, 1080 (2001).